



DIC Analysis of Prefabricated Fractured Coal Specimens under Stepwise Constant-Amplitude Cyclic Loading

Lei Wang

College of Energy Science and Engineering, Henan Polytechnic University, Jiaozuo, China

ABSTRACT

The mechanical response characteristics of coal-rock masses containing structural defects in mining roadways, under engineering disturbances, are prone to inducing dynamic instability phenomena in surrounding strata, such as roof collapse and rib spalling. These dynamic hazards pose a significant threat to the safe extraction of deep resources. Therefore, this paper takes coal-rock samples from Shendong mining area as the research object, designs stepwise constant-amplitude cyclic loading-unloading tests, and utilizes rock fatigue testing machine and DIC equipment to analyze in detail the strain field evolution process and final failure mode of prefabricated fractured coal samples under cyclic loading. The results demonstrate that prefabricated fractures play a significant controlling role in crack initiation, propagation and coalescence, and dominate the final failure mode of specimens.

KEYWORDS

Cyclic load; Defective coal sample; DIC.

1. INTRODUCTION

According to the spatiotemporal relationship between the gateway and the working face [1], gateways can be classified into solid coal gateways, coal mass-coal pillar gateways, and non-pillar gateways (gob-side entry driving and gob-side entry retaining) [2]. Throughout the entire lifecycle of the gateway, secondary fractures initiate and propagate in the surrounding rock under the influence of abutment pressure, gas drainage, and bolt drilling. Furthermore, periodic disturbances such as roof periodic fracturing [3], mechanical vibrations, and blasting [4] exacerbate fracture propagation, leading to reduced load-bearing capacity of the surrounding rock, bolt failure [5], and ultimately surrounding rock instability. Therefore, with the increasing intensity of coal mining, the rheological disturbance [6] and fatigue damage [7] of surrounding rock induced by cyclic loading cannot be ignored.

2. SAMPLE PREPARATION AND METHOD

2.1. Sample preparation

The raw coal blocks used in the test were collected from Shendong mining area, exhibiting intact structure, homogeneous texture and no visible fractures on the surface. In accordance with MT38-48-87 'Methods for Determining Physical and Mechanical Properties of Coal and Rock', the specimens were processed into standard cylindrical samples with a diameter of 50mm, height of 100mm, and end face flatness less than 0.02mm. According to relevant research findings, coplanar fractures exhibit the most significant influence on rock mass strength. Therefore, this study adopted pre-fabricated

fractures with an inclination angle of $\alpha=45^\circ$, length $2a=10\text{mm}$, and width $2b=0.5\text{mm}$ in the test specimens. As shown in Figure 1.



Figure 1. Sample specification

2.2. Test system

The tests were conducted using an RMT-150C electro-hydraulic servo-controlled rock testing system with a maximum axial load capacity of 100 kN. The axial displacement transducer had a maximum range of 5 mm. Force-controlled loading was applied at a rate of 1 kN/s. The tests employed a VIC-3DHS dynamic non-contact full-field strain measurement system, as shown in Figure 2. The VIC-3DHS is an advanced experimental measurement device that utilizes high-speed photography and digital image correlation (DIC) technology to measure full-field displacement and strain of materials or structures under static or dynamic loading. Developed by CSI (Correlated Solutions, Inc.) in the United States, this system is suitable for mechanical property testing of various materials, including rock, metal, plastic, composite materials, and biological tissues.



Figure 2. VIC-3D HS Dynamic Non-contact Full-field Strain Measurement System

2.3. Experimental design

The average peak strength σ of the specimens was determined through conventional uniaxial compression tests, which was then used to establish the upper and lower limits for the stepwise constant-amplitude cyclic loading tests. Starting from an initial stress of 0 MPa, cyclic loading was applied in increments of 20% of the average peak stress (σ), with cyclic upper limits set at 20%, 40%, 60%, and 80% of σ . The upper stress limit of each loading cycle served as the lower stress limit for the subsequent stress level. Based on field monitoring data of mining truck loads, blasting, and tunnel excavation, along with relevant research findings, a cyclic loading frequency of 0.2 Hz was adopted in this test. To investigate the repeated loading-unloading process experienced by coal under multi-step/mining disturbance, 20 cycles were applied at each stress level. The stress path of the designed stepwise constant-amplitude cyclic loading test is illustrated in Figure 3.

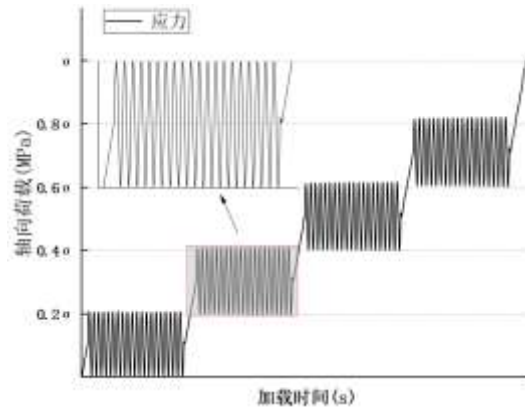
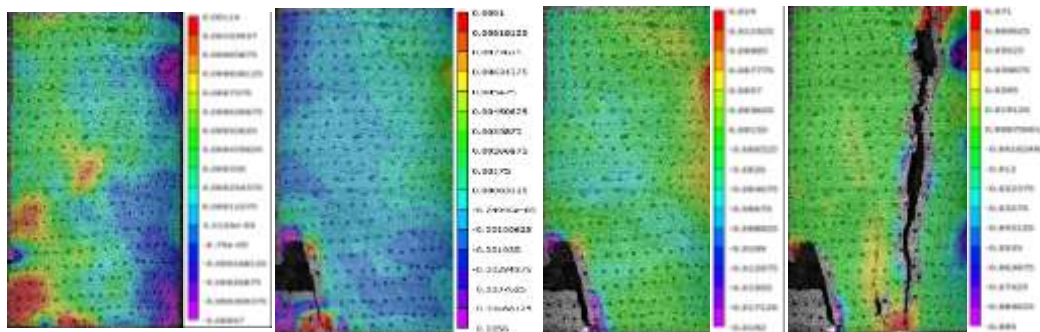


Figure 3. Axial load-time curve

3. DIC FEATURE ANALYSIS

3.1. Strain cloud map evolution analysis

Since most pre-cracked specimens underwent instantaneous crushing failure after completing the fourth loading cycle, the evolution process of radial strain fields (shown in Figure 4) was selected from the first to fourth cycles for analysis.



(a).Phase 1 of the cycle (b).Phase 2 of the cycle (c).Phase 3 of the cycle (d).Phase 4 of the cycle

Figure 4. Evolution process of radial strain nephogram of sample under constant amplitude cyclic loading by steps

As shown in Figure 4, during the initial loading stage, strain concentration primarily occurred at pre-existing micro-cracks in the specimen. With continued loading, cracks propagated along these micro-fractures, ultimately leading to specimen failure.

Under the influence of pre-existing fractures, Group B specimens exhibited strain concentration at the pre-crack locations during the first loading cycle. Red and green colors represent positive radial displacement (distributed on the left side of the specimen), while purple and blue indicate negative radial displacement (distributed on the right side). Under compressive loading, the specimen underwent expansion deformation on both sides without developing visible cracks. During the second loading cycle, the expansion deformation significantly diminished, indicating completion of the compaction stage and transition into the elastic deformation phase. A secondary crack initiated from the pre-existing fracture tip along the red-green boundary of the strain field in Figure 4(a) at the lower-left corner. Meanwhile, fracture closure in the upper-right corner transformed the originally purple negative radial displacement field into a green positive displacement field. During the third loading cycle, the secondary crack at the lower-left corner propagated further, while positive strain concentration occurred at the pre-existing fracture in the upper-right corner. In the fourth loading cycle, instead of developing cracks along the maximum strain field shown in Figure 4(c), a through-

going tensile crack formed on the specimen's right side. This failure pattern likely resulted from internal fracture propagation reaching the specimen surface.

3.2. Comparative analysis of failure mode characteristics

The crack propagation patterns were mapped based on strain nephograms as shown in Figure 5, revealing distinct differences between the two specimen types. During cyclic loading, Group A specimens generated multiple spalling zones due to specimen fragmentation. Group A specimens exhibited fewer visible surface cracks, developing only one shear crack in the spalling zone along with tensile cracks propagating along pre-existing micro-fractures, demonstrating a combined tensile-shear failure mode. Specimens in Group B exhibited not only the secondary crack propagating from the pre-existing fracture at the lower-left corner, but also a distinct tensile crack originating internally and extending outward, demonstrating a tensile failure mode.

Macroscopic failure morphology analysis demonstrates that pre-existing fractures exert significant control over crack initiation, propagation and coalescence, ultimately dominating the specimen's final failure mode. Specifically, cracks first initiate at the tips of pre-existing fractures. With increasing stress levels, secondary cracks progressively propagate and form coalescence zones near the pre-existing fractures, eventually connecting to cause complete specimen instability and failure.

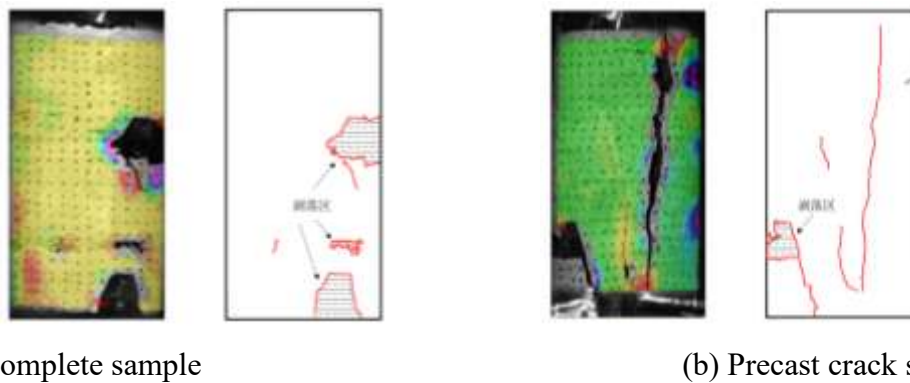


Figure 5. Crack distribution of two kinds of samples before crushing under stepped constant amplitude cyclic loading

4. SUMMARY

- (1) Pre-existing fractures exert significant control over crack initiation, propagation and coalescence.
- (2) Pre-existing fractures dominate the final failure mode of specimens, transforming the failure mechanism from tensile-shear composite failure to tensile failure.

REFERENCES

- [1] Zheng Jianwei, Ju Wenjun, Zhao Xi, et al. Analysis of the whole life cycle of stope and the spatiotemporal evolution characteristics of stress[J]. Journal of China Coal Society, 2019, 44(04): 995-1002
- [2] Xu Jialin, Qian Minggao, Shi Pingwu. Ground Pressure and Strata Control[M]. Xuzhou: China University of Mining and Technology Press, 2010.
- [3] Zhu Weibing, Yu Bin, Ju Jinfeng, et al. Experimental study on “transverse U-Y” periodic fracture characteristics of key strata in stope roof[J]. Coal Science and Technology, 2020, 48(02): 36-43.
- [4] An Tieliang. Fatigue damage of rock bolt anchoring body and principles of anti-fatigue support[D]. China University of Mining and Technology, 2021.
- [5] Jiao Jiankang. Impact failure mechanism and control technology of roadway bolting support structure under dynamic disturbance[D]. China Coal Research Institute, 2018.

- [6] Wang Bo, Ren Yongzheng, Tian Zhiyin, et al. Experimental study on sensitive neighborhood range of red sandstone under rheological disturbance effect[J]. Coal Science and Technology: 1-12.
- [7] Xing Luyi. Study on fatigue damage evolution mechanism and acoustic emission precursor characteristics of coal-rock under cyclic loading[D]. Shandong University of Science and Technology, 2019.